Robustness of the fractional topological phase to dephasing

R. A. Ribeiro,[1,*] A. A. Matoso,[1,2] L. E. Oxman,[3] A. Z. Khoury,[3] and S. Pádua[1]

[1]*Departamento de Física, Universidade Federal de Minas Gerais, 31270-901 Belo Horizonte, Minas Gerais, Brazil*
[2]*Institut für Angewandte Physik, Universität Bonn, Wegelerstrasse 8, 53115 Bonn, Germany*
[3]*Instituto de Física, Universidade Federal Fluminense, 24210-346 Niterói, Rio de Janeiro, Brazil*

In this work, we demonstrate theoretically via Kraus maps that the fractional topological phase in qudits is robust to phase noise. In our proposal, dephasing noise is inserted in an optical setup designed for measuring the fractional topological phase on photonic qudits encoded in path variables after local unitary operations are applied. Qudit states can be prepared with photon pairs generated by spontaneous parametric down-conversion crossing a multiple-slit array. Polarization as an additional degree of freedom and a two-photon longitudinal interferometer are the basic ingredients of the proposed setup. Although the visibility of the interference pattern decreases when noise is added, our calculation shows that the topological phase is preserved. This result stimulates further studies for the use of fractional topological phase in quantum gates due to its robustness in environments where phase noise is present.

I. INTRODUCTION

Two-qubit maximally entangled states (MESs) have been shown to be an interesting system for demonstrating the double-connectedness of the SO(3) rotation group [1]. This demonstration uses the one-to-one map between the group elements and the set of two-qubit MES [2–4]. It was shown that certain types of SU(2) ⊗ SU(2) cyclic transformations on two-qubit MES can reveal a topological property of the SO(3) ball by establishing a relation between the SO(3) topology and the global phase of a quantum state: the topological phase. The measurement of the topological phase for a two-qubit system was realized in different works [5–7]. In 2011, Oxman and Khoury [8] extended this discussion for qudit systems and showed that fractional topological phases (FTPs) appear in a two-qudit MES system undergoing a SU(d) ⊗ SU(d) cyclic evolution. An explicit description of the topological structure of the local SU(d) evolution in qudit bipartite systems was later presented in Ref. [9]. Recently, Khoury *et al.* [10] proposed an experiment to measure the FTPs in a two-qudit system by using two Mach-Zehnder interferometers. This phase was later measured with a conjugated Sagnac interferometer, an alternative and more stable setup than the original one proposed [11], and more recently with a hyperentangled photon source that provided higher fringe visibilities [12].

Geometric phase robustness to noise has been demonstrated theoretically by using adiabatic and nonadiabatic cyclic evolution of the quantum system [13–16]. This important result stimulates the search for quantum systems suitable for being used as geometric quantum gates and for geometric quantum computation [14,17–23]. Two-qudit topological phase evolution under dephasing noise was studied recently by using a master equation for treating the system-environment coupling [24].

In this work, we demonstrate theoretically via Kraus maps that the FTP is robust against the action of phase damping (dephasing in the photon path variables) when it is present in an interferometer suitable for measuring the two-qudit topological phase [10]. This result points in the direction of demonstrating the robustness of the fractional topological phase under dephasing in a concrete application. We organize this paper as follows.

In Sec. II, we introduce the concept of fractional topological phase as exposed in Ref. [10]. In Sec. III, we show how the phase noise is added in the original optical setup and calculate the evolution of the two-qudit state via Kraus maps including the experimental parameters used in Ref. [25]. In Sec. IV, we describe the FTP measurement process through the coincidence counts of correlated photon pairs, which give us a two-photon interference pattern. In Sec. V, we plot the theoretical interference patterns showing the expected phase shift between the initial and final interference patterns corresponding to the FTP with and without dephasing noise to compare with [10] curves. We draw our conclusions in Sec. VI.

II. FRACTIONAL TOPOLOGICAL PHASE FOR ENTANGLED QUDITS

Consider a bipartite system with discrete degrees of freedom represented by $|m\rangle$ and $|n\rangle$. In Einstein's sum notation, a two-qudit pure state can be written as

$$|\Psi_0\rangle = \alpha_{mn} |m, n\rangle. \tag{1}$$

For convenience, let us call the first qudit signal (*S*) and the second idler (*I*), referring to the photons generated by spontaneous parametric down-conversion (SPDC) prepared in qudit states, as described in the next sections. The state can be represented by a $d \times d$ matrix α with elements α_{mn}. Its norm and the internal product are given respectively by

_____
*rarbrasil@gmail.com

$\langle \psi | \psi \rangle = \text{Tr}[\alpha^\dagger \alpha]$ and $\langle \psi | \phi \rangle = \text{Tr}[\alpha^\dagger \beta]$ (β is the $d \times d$ matrix associated with ϕ). Local unitary qudit evolutions U_S and U_I lead to a state characterized by

$$\alpha' = U_S \alpha U_I^T. \tag{2}$$

By using the polar decomposition of a matrix, a general state can be parametrized in the form $\alpha = QU$, where Q is a (unique) positive semidefinite Hermitian matrix and $U \in U(d)$. The factor U, which is unique for invertible α's, can be further decomposed as $U = e^{i\phi} S$, where $S \in \text{SU}(d)$ and $e^{i\phi} = \sqrt[d]{\det U}$. The dth root is determined by the property $\sqrt[d]{e^{i\chi}} = e^{i\chi/d}$. Then, for time-varying unitary operations, we identify smooth and differentiable transformations on three sectors: $\phi \to \phi'$, $Q \to Q'$, and $S \to S'$, where $e^{i\phi'} = e^{i\phi}\sqrt[d]{\det U_S \det U_I}$, $Q' = \bar{U}_S Q \bar{U}_S^\dagger$, and $S' = \bar{U}_S S \bar{U}_I^T$. Here, $\bar{U}_S$ and $\bar{U}_I$ are the $\text{SU}(d)$ parts of the local unitary operations: $U_S = \sqrt[d]{\det U_S}\, \bar{U}_S$, and $U_I = \sqrt[d]{\det U_I}\, \bar{U}_I$.

Now, let us consider a cyclic evolution, that is, one where the final state is physically equivalent to the initial state. After an interval T, they only differ by a phase factor

$$\alpha(T) = e^{i\theta} \alpha(0). \tag{3}$$

By applying the polar decomposition on both sides,

$$e^{i\phi(T)} Q(T) S(T) = e^{i\theta} e^{i\phi(0)} Q(0) S(0), \tag{4}$$

we see that the phase θ is the sum of three components originated from each sector of the coefficients' matrix:

$$\theta = \Delta\phi + \gamma_Q + \gamma_S. \tag{5}$$

First we identify a trivial phase evolution $\phi(T) = \phi(0) + \Delta\phi$ from sector U(1), which has contributions from signal and idler, $\phi = \phi_S + \phi_I$. From the sector of positive definite Hermitian matrices, if we write $Q(T) = e^{i\gamma_Q} Q(0)$, the condition of hermiticity imposes that $\gamma_Q = 0$. Finally, in the $\text{SU}(d)$ sector we have $S(T) = e^{i\gamma_S} S(0)$, where using the matrix determinant property $\det S(T) = e^{id\gamma_S} \det S(0)$ and the fact that $S(T), S(0) \in \text{SU}(d)$, we obtain the fractional phase

$$\gamma_S = \frac{2n\pi}{d} = \theta - \Delta\phi \quad (n = 1, 2, \ldots, d-1). \tag{6}$$

This corresponds to the difference between the global and the trivial phases. Therefore, only fractional phases from the $\text{SU}(d)$ sector arise and the nature of this phase is purely topological. This is due to the fact that the set of $\text{SU}(d)$ matrices S with the identification $S(T) \equiv e^{i\gamma_S} S(0)$ is represented by a nonsimply connected manifold. It is noteworthy that the $\text{SU}(d)$ manifold without the identification is simply connected.

The fractional topological phase (FTP) is measured from the phase difference between two displaced interference patterns, as Aharonov and Anandan wrote in a similar experimental purpose for the geometrical phase measurement [26]: "Then the phase difference between the two beams is just the geometrical phase, which is observable in principle, **from the interference pattern**, even when the magnetic field is varied nonadiabatically." In Berry's words [27], "This phase factor is observable by interference if the cycled system is recombined with another that was separated from it at an earlier time and whose Hamiltonian was kept constant." In the next sections we introduce the FTP measurement experiment with dephasing noise in a quantum optical setup.

III. DEPHASING MAPS ON SPATIALLY ENCODED QUDITS

A. Spatial encoding of qudits

Consider the interferometer shown in Fig. 1. Two noncollinear beams of entangled horizontally polarized photons, named signal (S) and idler (I), are generated in a nonlinear crystal by SPDC [28]. Each photon beam passes through one of the two identical multiple-slit masks (d slits), preparing the photon pair in a two-qudit state on their transverse path degree of freedom. Therefore we can write

$$|\Psi_0\rangle = \alpha_{mn} |mH, nH\rangle, \tag{7}$$

where $m, n = 1, 2, \ldots, d$, α_{mn} is the probability amplitude of having one signal photon (S) passing through the slit m and one idler photon (I) passing through the slit n. For notation simplicity, we use in this article the Einstein summation convention. After the slits, two half-wave plates rotate the photons polarization by $45°$, and the initial quantum state is transformed to

$$|\Psi_0\rangle = \alpha_{m\mu, n\nu} |m\mu, n\nu\rangle, \tag{8}$$

where $\alpha_{m\mu, n\nu} = \alpha_{mn}\alpha_{\mu,\nu}$, with $\alpha_{\mu,\nu} = 1/2$ and $\mu, \nu = H$ or V. The state density operator is then given by

$$\rho_{SI} = \frac{\alpha_{m\mu, n\nu}\alpha^*_{m'\mu', n'\nu'}}{4} |m\mu, n\nu\rangle \langle m'\mu', n'\nu'|. \tag{9}$$

This is the state just before the two Mach-Zehnder interferometer entrances. Phase noise and unitary operations are
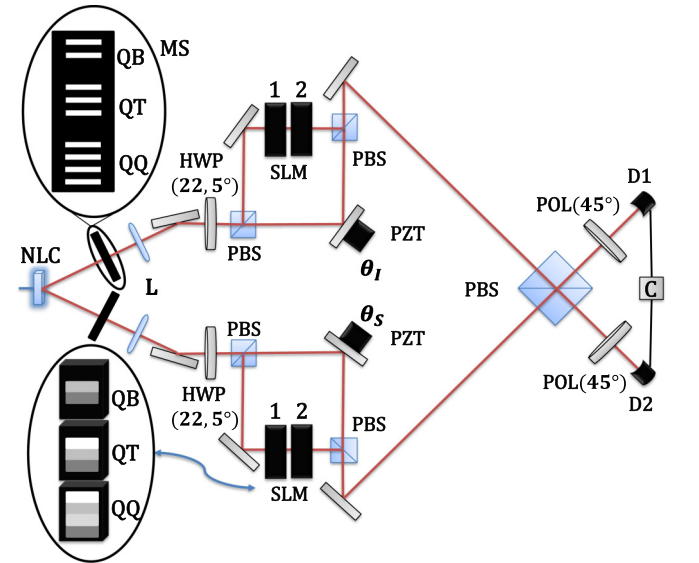

FIG. 1. Experimental proposal for measuring the fractional topological phase in a two-qudit photonic system in the presence of dephasing. Idler (I) and signal (S) photons are generated through spontaneous parametric down-conversion. NLC is a nonlinear crystal and each multiple-slit (MS) mask has d apertures. HWP is a half-wave plate. SLM is a spatial light modulator. L indicates a pair of lenses that project the image of the slits to the SLMs. PBS is a polarizing beam splitter. POL is a polarizer, θ_j ($j = S$ and I) is a path phase added by the displacement of the mirror coupled to piezoelectric ceramic (PZT), and D_l ($l = 1$ and 2) is a single-photon detector.

then applied to the photon path degrees of freedom inside the interferometers conditioned to the photon polarization. Suitable unitary operations will transform the input state and generate the FTP in the transformed state. We refer to the unitary operation leading to the FTP as the "FTP operation". The phase noise and the FTP operations can be performed by the spatial light modulators (SLM) positioned within the two Mach-Zehnder interferometer built with input and output polarizing beam splitters (PBSs). The SLMs are controlled externally by a computer that changes the voltage on a desired region of the liquid crystal display placed in the path of the photons, thus varying the phases added to them. In this way, it can insert different phases on each transversal path mode labeled by m and n. The applied operations to the photon path degrees of freedom are represented by Kraus operators [29].

Let the Kraus operators that apply a transformation on the path of each photon be conditioned to the polarization. This operation is feasible, because the horizontal (H) and vertical (V) polarization components of each photon are separated in the arms of a Mach-Zehnder interferometer. They are written as

$$K_{hj}^{SI} = \left(K_{h\alpha}^S \otimes |\alpha\rangle \langle\alpha|\right) \otimes \left(K_{j\beta}^I \otimes |\beta\rangle \langle\beta|\right), \quad (10)$$

where K^S and K^I act over the signal and idler spatial subspace, respectively, and the projectors act over the polarization subspace ($\alpha, \beta = H$ or V). They implement the following map that acts on the pure state density matrix shown in Eq. (9):

$$\varepsilon_K(\rho_{SI}) = p_{hj} K_{hj}^{SI} \rho_{SI} K_{hj}^{SI\dagger}, \quad (11)$$

where $p_{hj} K_{hj}^{SI\dagger} K_{hj}^{SI} \leqslant \hat{I}$, $\hat{I}$ is the identity operator and $\sum_{h,j} p_{hj} = 1$, with $h, j = 0, 1, \ldots, d$. The initial pure state is transformed to a mixed state weighted by p_{hj}, which is the classical probability that gives different weights for the different Kraus operators. The term p_{00} is the probability that the identity operator $\hat{I}$ acts on the initial state and $p_{hj\neq00}$ are the probabilities that the initial state is transformed by the other Kraus operators.

The operators performing the FTP operation in a Mach-Zehnder are represented by the following diagonal unitary matrices:

$$U_S = e^{i\phi_p(t_S)}|p\rangle \langle p|, \quad U_I = e^{i\chi_q(t_I)}|q\rangle \langle q|, \quad (12)$$

where ϕ_p and χ_q are the phases added to the transversal path states of S ($|p\rangle$) and I ($|q\rangle$) photons during the evolution parametrized by t_S and t_I. Notice that $U_S^\dagger U_S = \hat{I}$ and $U_I^\dagger U_I = \hat{I}$. We can represent these operators by a Kraus operator that can be expressed similarly to Eq. (10) as

$$T_{SI} = \left(e^{i\phi_p \delta_\alpha^V}|p\rangle \langle p| \otimes |\alpha\rangle \langle\alpha|\right)_S \otimes \left(e^{i\chi_q \delta_\beta^V}|q\rangle \langle q| \otimes |\beta\rangle \langle\beta|\right)_I, \quad (13)$$

where $T^\dagger T = \hat{I}$ and δ_i^j is Kronecker δ that is 1 for $i = j$ and 0 for $i \neq j$. The Kronecker δ function in Eq. (13) guarantees that there is no phase addition if the photon polarization is horizontal and that there is the addition of the phases implementing the FTP operation if the photon polarization is vertical. By using Eq. (11) we obtain the transformed density matrix from Eq. (9). If the Kraus operator given in Eq. (13) is

used we obtain the state

$$\varepsilon_T(\rho_{SI}) = \frac{\alpha_{m\mu,n\nu} \alpha_{m'\mu',n'\nu'}^*}{4} |m\mu, n\nu\rangle \langle m'\mu', n'\nu'|$$
$$\times e^{i(\phi_m \delta_\mu^V + \chi_n \delta_\nu^V)} e^{-i(\phi_{m'} \delta_{\mu'}^V + \chi_{n'} \delta_{\nu'}^V)}. \quad (14)$$

B. Dephasing maps

Now consider a specific phase noise called dephasing which is also added to the photons path conditioned to the vertical polarization [30]. This dephasing operation is represented by the following Kraus operators:

$$D_{hj}^{SI} = \left(e^{i\pi \delta_p^h \delta_\alpha^V}|p\rangle \langle p| \otimes |\alpha\rangle \langle\alpha|\right)_S \otimes \left(e^{i\pi \delta_q^j \delta_\beta^V}|q\rangle \langle q| \otimes |\beta\rangle \langle\beta|\right)_I, \quad (15)$$

where $D_{hj}^{SI\dagger} D_{hj}^{SI} = \hat{I}$ and $h, j = 0, 1, \ldots, d$. The dephasing noise can be added to the photons' transversal paths by the second SLM (SLM2) shown in Fig. 1, following the experimental strategy discussed in Ref. [25]. Applying the dephasing Kraus operators on the state described by $\varepsilon_T(\rho_{SI})$, we find

$$\varepsilon_D[\varepsilon_T(\rho_{SI})] = e^{i[(\pi\delta_m^h + \phi_m)\delta_\mu^V + (\pi\delta_n^j + \chi_n)\delta_\nu^V]} \rho_{SI} p_{hj}$$
$$\times e^{-i[(\pi\delta_{m'}^h + \phi_{m'})\delta_{\mu'}^V + (\pi\delta_{n'}^j + \chi_{n'})\delta_{\nu'}^V]}, \quad (16)$$

which is a mixture of pure states weighted by p_{hj}. Note that the original state ρ_{SI} still appears in the expression but it is now modified.

The topological phase is measured by varying two independent phases in the interferometer and measuring the interference pattern with and without the local unitary operations applied to the two-qudit path state. The fractional topological phase is measured from the shift in the interference patterns. The phase scanning operations (which add θ_S and θ_I to the signal and idler paths, respectively) are realized by the mirrors coupled to piezoelectric transducers (PZTs) in one of the arms of the Mach-Zehnders (Fig. 1). This operation can be expressed as

$$S = \left(e^{i\theta_S \delta_\alpha^H} I_{\text{path}} \otimes |\alpha\rangle \langle\alpha|\right)_S \otimes \left(e^{i\theta_I \delta_\beta^H} I_{\text{path}} \otimes |\beta\rangle \langle\beta|\right)_I, \quad (17)$$

with $S^\dagger S = \hat{I}$. Finally, taking into account all the quantum operations applied to the input state in the Mach-Zehnder interferometers, represented by $\varepsilon(\rho_{SI}) = \varepsilon_S \circ \varepsilon_D \circ \varepsilon_T(\rho_{SI})$, we obtain the final transformation of the initial density operator as

$$\varepsilon(\rho_{SI}) = p_{hj} F_{m\mu,n\nu}^{hj} F_{m'\mu',n'\nu'}^{hj*} |m\mu, n\nu\rangle \langle m'\mu', n'\nu'|, \quad (18)$$

where

$$F_{m\mu,n\nu}^{hj} = \frac{\alpha_{m\mu,n\nu}}{2} e^{i\{[(\pi\delta_m^h + \phi_m)\delta_\mu^V + \theta_S \delta_\mu^H] + [(\pi\delta_n^j + \chi_n)\delta_\nu^V + \theta_I \delta_\nu^H]\}}. \quad (19)$$

The final density operator describes a system whose state is a mixture of pure states weighted by the classical probabilities p_{hj} and by the final amplitudes $F_{m\mu,n\nu}^{hj}$, according to

$$\varepsilon(\rho_{SI}) = p_{hj} |\psi_{hj}\rangle \langle\psi_{hj}|, \quad (20)$$

where

$$|\psi_{hj}\rangle = F_{m\mu,n\nu}^{hj} |m\mu, n\nu\rangle. \quad (21)$$

It is useful to decompose the density matrix elements of the evolved density operator [Eq. (18)] in three distinct parts: one part corresponding to the initial amplitudes ($\alpha_{m\mu,n\nu}/2$), another one responsible for a positive or negative sign in

the density matrix elements as a consequence of adding the dephasing noise ($D_{m\mu,n\nu}^{hj}$), and the last part composed by the unitary operation and the scanning phase factors ($f_{m\mu,n\nu}$). Then, we can rewrite the pure state amplitudes as

$$F_{m\mu,n\nu}^{hj} = \tfrac{1}{2} \alpha_{m\mu,n\nu} D_{m\mu,n\nu}^{hj} f_{m\mu,n\nu}, \tag{22}$$

where

$$D_{m\mu,n\nu}^{hj} = e^{i\pi(\delta_m^h \delta_\mu^V + \delta_n^j \delta_\nu^V)} = (-1)^{(\delta_m^h \delta_\mu^V + \delta_n^j \delta_\nu^V)},$$

$$f_{m\mu,n\nu} = e^{i[(\phi_m \delta_\mu^V + \theta_S \delta_\mu^H) + (\chi_n \delta_\nu^V + \theta_I \delta_\nu^H)]}. \tag{23}$$

Equation (22) shows us that the phase factors $f_{m\mu,n\nu} f_{m'\mu',n'\nu'}^*$ are identical for all components of the sum over h and j in the mixed state. Note that if we remove the dephasing noise from the interferometers ($p_{hj} D_{m\mu,n\nu}^{hj} D_{m'\mu',n'\nu'}^{hj*} = 1$) and make explicit the polarization components [Eq. (8)] we recover the state studied by Khoury *et al.* [10]:

$$|\Psi\rangle = \frac{\alpha_{m,n}}{2} \big[e^{i(\theta_S + \theta_I)} |mH, nH\rangle + e^{i(\theta_S + \chi_n)} |mH, nV\rangle$$

$$+ e^{i(\phi_m + \theta_I)} |mV, nH\rangle + e^{i(\phi_m + \chi_n)} |mV, nV\rangle \big]. \tag{24}$$

Equation (18) indicates that we obtain the same final state by exchanging the operators' order and therefore by exchanging the quantum operations in the Mach-Zehnder interferometers. Indeed, it is important to remember that the path dephasing does not produce photon losses and that the dephasing effect will only result in decreased visibilitiy of the interference pattern used to measure the fractional topological phase.

The results presented here can be obtained by a setup similar to the one shown in Fig. 1, but without the two Mach-Zehnders. The use of Mach-Zehnders is pedagogical, but for practical purposes they can be substituted by a phase-shifter inside a Sagnac interferometer as shown in Ref. [11], replacing the PZT to introduce the phases θ_s and θ_i between the component H and V of the state. It is important to remember that the SLM acts only in one polarization component, either H or V, depending on the SLM's orientation axis. From the theoretical point of view, this change does not have fundamental impact. However, the use of a Sagnac interferometer can be better in the experimental implementation for being more stable.

IV. SPATIAL QUANTUM CORRELATIONS UNDER DEPHASING

We follow below the steps shown in Ref. [10] for obtaining the coincidence rate at the exit of the interferometer shown in Fig. 1. The positive frequency components of the signal and idler vector field operators are

$$\mathbf{E}_S^+ = E_{SH}^+ \widehat{e}_H + E_{SV}^+ \widehat{e}_V, \quad \mathbf{E}_I^+ = E_{IH}^+ \widehat{e}_H + E_{IV}^+ \widehat{e}_V, \tag{25}$$

where $\widehat{e}_\mu$ ($\mu = V$ or H) is the unit vector along the direction of the vertical (V) or horizontal (H) polarization. Each component is expanded in terms of the slit modes η and the annihilation operators a and b as

$$E_{S\mu}^+ = a_{p\mu} \eta_P(\mathbf{r_S}), \quad E_{I\nu}^+ = b_{q\nu} \eta_q(\mathbf{r_I}), \tag{26}$$

where $\mathbf{r_j}$ ($\mathbf{j = S}$ and $\mathbf{I}$) are the signal and idler position variables. The slit modes refer to the field spatial distribution

transmitted through the different slits. Each function η_p (η_q) is the projection of the slit state (photon path state in the slit spatial mode) over the continuous spatial Hilbert space $\eta_m(\mathbf{r}) = \langle x|m\rangle$, such that the orthogonality condition

$$\int d^2\mathbf{r} \, \eta_m^*(\mathbf{r})\eta_m(\mathbf{r}) = \delta_{mn} \tag{27}$$

is valued. The operators $a_{p\mu}$ and $b_{q\nu}$ are the annihilation operators acting in the usual way on two-photon states $|m\sigma, n\epsilon\rangle$ representing one signal photon passing through slit m with σ polarization and one idler photon passing through slit n with ϵ polarization. The action of the annihilation operators reads

$$a_{p\mu}b_{q\nu} |m\sigma, n\epsilon\rangle = \delta_{pm}\delta_{\mu\sigma} \delta_{qn}\delta_{\nu\epsilon} |\text{vac}\rangle, \tag{28}$$

where $|\text{vac}\rangle$ is the vacuum state meaning no photon is transmitted through the slit m or n. After transmission through the final PBS, the field operators at the detectors planes are

$$E_1^+ = \frac{1}{\sqrt{2}}(iE_{SV}^+ + E_{IH}^+), \quad E_2^+ = \frac{1}{\sqrt{2}}(E_{SH}^+ + iE_{IV}^+). \tag{29}$$

The coincidence count function at the exit of the PBS is given by

$$C(\mathbf{r_1}, \mathbf{r_2}) = \text{Tr}[E_2^+ E_1^+ \rho E_1^- E_2^-], \tag{30}$$

where $E_j^- = (E_j^+)^\dagger$ ($j = 1$ or 2). By using the density matrix given by Eq. (22) and the action of the annihilation operators according to Eq. (28), we obtain the coincidence counts from Eq. (30):

$$C(\mathbf{r_1}, \mathbf{r_2}) = p_{hj} \big(F_{mH,nH}^{hj} F_{m'H,n'H}^{hj*} \; \eta_m^2 \eta_n^1 \eta_{m'}^{2*} \eta_{n'}^{1*}$$

$$+ F_{mV,nV}^{hj} F_{m'V,n'V}^{hj*} \; \eta_n^2 \eta_m^1 \eta_{n'}^{2*} \eta_{m'}^{1*}$$

$$- F_{mH,nH}^{hj} F_{m'V,n'V}^{hj*} \; \eta_m^2 \eta_n^1 \eta_{n'}^{2*} \eta_{m'}^{1*}$$

$$- F_{mV,nV}^{hj} F_{m'H,n'H}^{hj*} \; \eta_n^2 \eta_m^1 \eta_{n'}^{2*} \eta_{m'}^{1*} \big)/4. \tag{31}$$

We are only interested in the phase originated from the local operations [Eq. (12)] on the qudits. Since the slit modes are orthonormal, the integration in the transversal spatial variables of the coincidence counts eliminates the spatial interference between different slit modes and it will show only the Mach-Zehnder longitudinal interference in the two-photon correlation. This integration corresponds experimentally to the use of large-aperture detectors, insensitive to the detailed spatial structure of the two-photon quantum correlations. However, the Hilbert space dimension remains manifested through the two-qudit coefficients in the integrated coincidence function. The coincidence count calculated through the integration of Eq. (31), considering the orthonormality condition Eq. (27), is

$$C \equiv \int d^2\mathbf{r_1}d^2\mathbf{r_2} C(\mathbf{r_1}, \mathbf{r_2})$$

$$= \frac{p_{hj}}{4} \big(F_{mH,nH}^{hj} F_{mH,nH}^{hj*} + F_{mV,nV}^{hj} F_{mV,nV}^{hj*} - F_{mH,nH}^{hj} F_{nV,mV}^{hj*}$$

$$- F_{mV,nV}^{hj} F_{nH,mH}^{hj*} \big). \tag{32}$$

Remembering that $\alpha_{m\mu,n\nu} = \alpha_{m,n}\alpha_{\mu,\nu}$ ($\mu, \nu = H$ or V) and using Eq. (19), we can work out the integrated coincidence count to find

$$C = \tfrac{1}{16} \big[2 - \alpha_{m,n}\alpha_{n,m}^* p_{hj} \big(f_{m,n}^{hj} + f_{n,m}^{hj*} \big) \big], \tag{33}$$

where

$$f_{m,n}^{hj} \equiv (-1)^{(\delta_m^h + \delta_n^j)} e^{i[(\phi_m + \chi_n) - (\theta_S + \theta_I)]},$$

$$f_{n,m}^{hj*} \equiv (-1)^{(\delta_n^h + \delta_m^j)} e^{-i[(\phi_n + \chi_m) - (\theta_S + \theta_I)]}. \quad (34)$$

This is the coincidence count at the exit of the PBS placed before the detectors (Fig. 1) in the scheme proposed to measure the fractional topological phase of qudits in a dephasing environment.

We use Eq. (33) in the next section for comparing the fractional topological phase of qudits which can be measured from the interferometer shown in Fig. 1 without and with dephasing noise. Note that the normalized coincidence count given by Eq. (33) is limited to 1/4. This is so because of the polarizers filtering before the detectors and the signal loss due to events where signal and idler photons exit the final PBS through the same output port and do not produce a coincidence. Therefore, in the examples shown below, we multiply Eq. (33) by 4 to make the interference patterns oscillate in the interval between 0 and 1 when maximal visibility is attained.

Our final results are limited to diagonal operations, but it is possible to change Eq. (15) including new terms that represent an off-diagonal operation and redo the calculation. We chose to study the noise diagonal operations at first because their experimental implementation for slit states is straightforward with the use of spatial light modulators. It is possible to use different noise environments, such as amplitude damping, in a way similar to that done above.

V. NUMERICAL RESULTS

In the next steps we refer to the setup with no dephasing and the results from Ref. [10] to compare the cases with and without noise.

Consider two photonic qubits ($d = 2$), qutrits ($d = 3$), or ququarts ($d = 4$) under their respective signal and idler unitary diagonal operations

$$U_S = \text{diag}[e^{i\phi_1}, e^{i\phi_2}, \ldots, e^{i\phi_d}],$$
$$U_I = \text{diag}[e^{i\chi_1}, e^{i\chi_2}, \ldots, e^{i\chi_d}]. \quad (35)$$

As shown in Ref. [10], the coincidence counts at the exit of the interferometer used to measure FTP shift is proportional to

$$C = \sum_{m,n} |\alpha_{m,n}|^2 \cos^2 \left[\frac{\phi_m + \chi_n - \theta}{2} \right], \quad (36)$$

where it was considered $\theta = \theta_S + \theta_I - \pi$. The following phases are used in the local operations [Eq. (35)] and are supposed to be applied to the photonic qudit path states ($d = 2, 3,$ or 4) by the SLMs [10]:

$$d = 2 \begin{cases} \phi_1 = \chi_1 = \frac{\pi}{2}t, \\ \phi_2 = \chi_2 = -\frac{\pi}{2}t, \end{cases}$$

$$d = 3 \begin{cases} \phi_1 = \chi_1 = \frac{2\pi}{3}t - \frac{\pi}{3}(2t-1)H\left(t - \frac{1}{2}\right), \\ \phi_2 = \chi_2 = -\frac{2\pi}{3}t, \\ \phi_3 = \chi_3 = \frac{\pi}{3}(2t-1)H\left(t - \frac{1}{2}\right), \end{cases}$$

$$d = 4 \begin{cases} \phi_1 = \chi_1 = -\frac{\pi}{4}t + \frac{\pi}{2}(1-2t)H\left(t - \frac{1}{2}\right), \\ \phi_2 = \chi_2 = \frac{\pi}{4}t, \\ \phi_3 = \chi_3 = \frac{3\pi}{4}t - \frac{\pi}{2}(1-2t)H\left(t - \frac{1}{2}\right), \\ \phi_4 = \chi_4 = -\frac{3\pi}{4}t, \end{cases} \quad (37)$$

in which t is a real parameter, $t \in [0, 1]$, and $H(t)$ is the Heaviside function

$$H(x) = \begin{cases} 0, & \text{if } x < 0; \\ \frac{1}{2}, & \text{if } x = 0; \\ x, & \text{if } x > 0. \end{cases} \quad (38)$$

Equation (37) describes a continuous evolution of the phases in each slit mode which produces an SU(d) local evolution applied on each qudit independently. However, the FTP phase is extracted from the phase shift obtained from the displacement of the interference pattern at $t = 1$ relative to the $t = 0$ interference pattern. Then, it is sufficient to calculate the coincidence counts in terms of θ for a few particular t values like the ones shown in Table I. The interference visibility vanishes at $t = 1/2$ for the MES. This means that at $t = 1/2$ the evolved qudit state is orthogonal to the initial state ($t = 0$). This feature will be checked with the following MESs for qubits ($d = 2$), qutrits ($d = 3$), and ququarts ($d = 4$),

$$|\varphi_{\text{mes}}\rangle = \frac{1}{\sqrt{2}}(|11\rangle + |22\rangle),$$

$$|\varphi_{\text{mes}}\rangle = \frac{1}{\sqrt{3}}(|11\rangle + |22\rangle + |33\rangle),$$

$$|\varphi_{\text{mes}}\rangle = \frac{1}{\sqrt{4}}(|11\rangle + |22\rangle + |33\rangle + |44\rangle), \quad (39)$$

and compared with the following product states (PSs),

$$|\varphi_{\text{ps}}\rangle = \frac{1}{2}(|1\rangle + |2\rangle) \otimes (|1\rangle + |2\rangle),$$

$$|\varphi_{\text{ps}}\rangle = \frac{1}{3}(|1\rangle + |2\rangle + |3\rangle) \otimes (|1\rangle + |2\rangle + |3\rangle),$$

$$|\varphi_{\text{ps}}\rangle = \frac{1}{4}(|1\rangle + |2\rangle + |3\rangle + |4\rangle) \otimes (|1\rangle + |2\rangle + |3\rangle + |4\rangle). \quad (40)$$

TABLE I. Phase values given by Eq. (37) for $t = 0$, 1/2, and 1. Note that $t = 0$ and $t = 1$ correspond to the initial and final instants of the two-qudit SU(d) operations for $d = 2$, $d = 3$, and $d = 4$. The FTP is obtained from the shift of the interference pattern when t varies from 0 to 1.

Principal phases			
t	$\phi_1 = \chi_1$	$\phi_2 = \chi_2$	
0	0	0	
$\frac{1}{2}$	$\pi/4$	$-\pi/4$	
1	$\pi/2$	$-\pi/2$	
t	$\phi_1 = \chi_1$	$\phi_2 = \chi_2$	$\phi_3 = \chi_3$
0	0	0	0
$\frac{1}{2}$	$\pi/3$	$-\pi/3$	0
1	$\pi/3$	$-2\pi/3$	$\pi/3$
t	$\phi_1 = \chi_1$	$\phi_2 = \chi_2$	$\phi_3 = \chi_3$	$\phi_4 = \chi_4$
0	0	0	0	0
$\frac{1}{2}$	$-\pi/8$	$\pi/8$	$3\pi/8$	$-3\pi/8$
1	$-5\pi/4$	$\pi/4$	$7\pi/4$	$-3\pi/4$

TABLE II. Expressions for the two-photon interference patterns given by Eq. (33) for the two-qudit maximally entangled (MES) and product (PS) states with $d = 2$, 3, and 4, when the local SU(d) operations shown in Eq. (35) are applied. The parameter values $t = 0$, $1/2$, and 1 are considered. Two-qudit states are in a dephasing environment determined by parameter $p \in [0, 1]$. The visibilities v_{ps} and v_{mes} for product and maximally entangled states are presented.

	FTP calculation under dephasing	
t	$C_{mes}(p)$ ($d = 2$)	v_{mes}
0	$\frac{1}{2} - \frac{(-1+p)^2}{2}\cos(\theta)$	$(-1+p)^2$
$\frac{1}{2}$	$\frac{1}{2}$	0
1	$\frac{1}{2} - \frac{(-1+p)^2}{2}\cos(\theta - \pi)$	$(-1+p)^2$
t	$C_{ps}(p)$ ($d = 2$)	v_{ps}
0	$\frac{1}{2} - \frac{(-1+p)^2}{2}\cos(\theta)$	$(-1+p)^2$
$\frac{1}{2}$	$\frac{1}{2} - \frac{(-1+p)^2}{4}\cos(\theta)$	$\frac{(-1+p)^2}{2}$
1	$\frac{1}{2}$	0
t	$C_{mes}(p)$ ($d = 3$)	v_{mes}
0	$\frac{1}{2} - \frac{(3-2p)^2}{18}\cos(\theta)$	$\frac{(3-2p)^2}{9}$
$\frac{1}{2}$	$\frac{1}{2}$	0
1	$\frac{1}{2} - \frac{(3-2p)^2}{18}\cos(\theta - \frac{2\pi}{3})$	$\frac{(3-2p)^2}{9}$
t	$C_{ps}(p)$ ($d = 3$)	v_{ps}
0	$\frac{1}{2} - \frac{(3-2p)^2}{18}\cos(\theta)$	$\frac{(3-2p)^2}{9}$
$\frac{1}{2}$	$\frac{1}{2} - \frac{2(3-2p)^2}{81}\cos(\theta)$	$\frac{4(3-2p)^2}{81}$
1	$\frac{1}{2} - \frac{(3-2p)^2}{162}\cos(\theta - \frac{2\pi}{3})$	$\frac{(3-2p)^2}{81}$
t	$C_{mes}(p)$ ($d = 4$)	v_{mes}
0	$\frac{1}{2} - \frac{(-2+p)^2}{8}\cos(\theta)$	$\frac{(-2+p)^2}{4}$
$\frac{1}{2}$	$\frac{1}{2}$	0
1	$\frac{1}{2} - \frac{(-2+p)^2}{8}\cos(\theta - \frac{\pi}{2})$	$\frac{(-2+p)^2}{4}$
t	$C_{ps}(p)$ ($d = 4$)	v_{ps}
0	$\frac{1}{2} - \frac{(-2+p)^2}{8}\cos(\theta)$	$\frac{(-2+p)^2}{4}$
$\frac{1}{2}$	$\frac{1}{2} - \frac{2(2+\sqrt{2})(-2+p)^2}{128}\cos(\theta)$	$\frac{(2+\sqrt{2})(-2+p)^2}{32}$
1	$\frac{1}{2} - \frac{(-2+p)^2}{32}\cos(\theta - \frac{\pi}{2})$	$\frac{(-2+p)^2}{16}$

If we substitute the phases shown in Table I into Eq. (33) for the MESs and the PSs [Eqs. (39) and (40)], we are able to compute the FTP for the state evolution under local SU(d) operations in the presence of dephasing. In Table II we present the calculated coincidence counts. The notation $C_{mes}(p)$ and $C_{ps}(p)$ are used for the coincidence counts for the cases of maximally entangled and product qudit states ($d = 2$, $d = 3$, and $d = 4$), respectively. In Eq. (11), we consider local iso-weighted dephasing for each photon, i.e., $p_{hj} = p_h \times p_j$, $p_{h\neq 0} = p_{j\neq 0} = p/d$, and $p_0 = 1 - p$. The parameter p determines the weight of dephasing relative to the identity operation. The visibility of the interference pattern will be calculated as $v = (C_{max} - C_{min})/(C_{max} + C_{min})$. When $p = 0$ in the equations shown in Table II, we recover the result given by Eq. (36) for the case without phase noise, as expected [10].
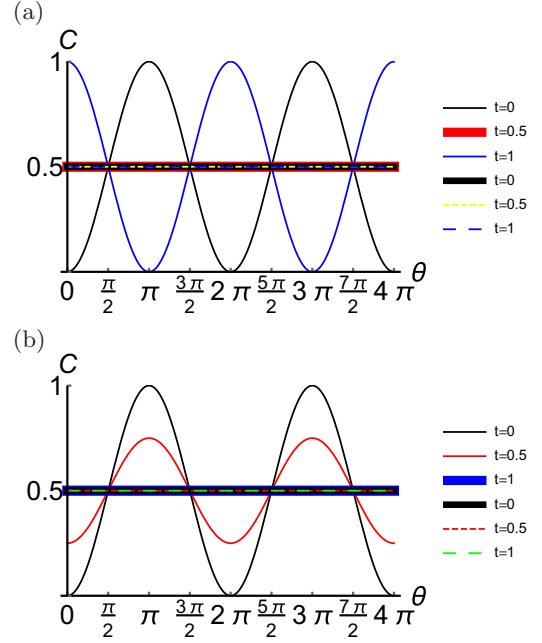

FIG. 2. Interference patterns for measuring the fractional topological phase of two-qubits states: (a) maximally entangled state and (b) product state. Coincidence rates (C) at the exit of the final PBS shown in Fig. 1 are plotted in terms of θ for photons prepared in two-qubit maximally entangled and product states. The corresponding expressions are presented in Table II. The curves that correspond to the first three labels shown on the right of each set of graphs, $t = 0$ (black continuous curves), $t = 0.5$ (red continuous thick and thin curves), and $t = 1$ (blue continuous thick and thin curves), are calculated for $p = 0$ (no phase noise present). The curves that correspond to the remaining three labels, $t = 0$ (black continuous thick curves), $t = 0.5$ (yellow and red shortdashed curves), and $t = 1$ (blue and green dashed curves), are calculated for $p = 1$ (100% dephasing present). The π interference pattern displacement between $t = 0$ and $t = 1$ SU(d) operations for $p = 0$ correspond to the predicted FTP for the maximally entangled two-qubit states. The visibility goes to zero at $t = 0.5$ for MES because the evolved state for $t = 0.5$ is the orthogonal to the initial state and the two-qubit state is the only case in which the visibility is null under 100% dephasing ($p = 1$).

Let us analyze the expressions presented in Table II. Except for the two-qubit product state, the $2\pi/d$ shift is present in all cases between $t = 0$ and $t = 1$ interference patterns, although the visibility falls in the two-qudit ($d > 2$) product state. This occurs even for $p = 1$ (100% of dephasing). These results show us that the $2\pi/d$ shift under local SU(d) operations in the presence of dephasing is very robust.

Figures 2–4 show plots of the coincidence expressions displayed in Table II for $p = 0$ (no dephasing) and $p = 1$ (maximum dephasing) for the maximally entangled and product states when $t = 0$, $1/2$, and 1.

The visibility of the interference patterns vanish at $t = 1/2$ for the MES, which means that the evolved state for $t = 1/2$ is orthogonal to the initial state. Another significant aspect with MESs is the complete recovery of the initial visibility at the end of the cyclic SU(d) $\otimes$ SU(d) evolution ($t = 1$). The two-qubit case is the only one in which the visibility goes to zero under 100% dephasing (Fig. 2). For the product states
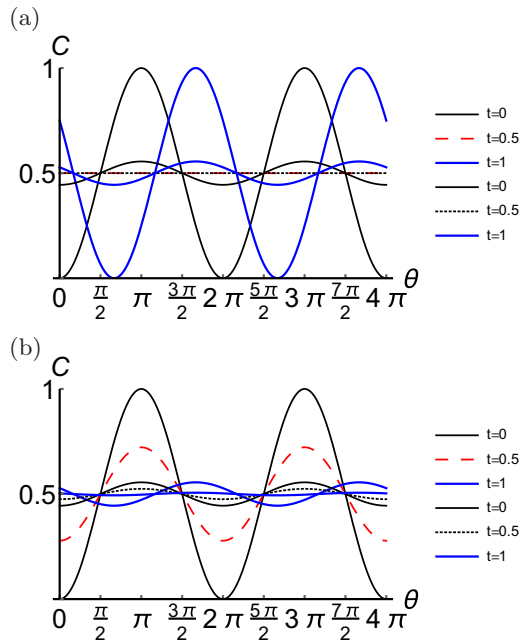
(a)

(b)

FIG. 3. Situation analogous to Fig. 2 for two-qutrit states: (a) maximally entangled state and (b) product state. The curves that correspond to the first three labels shown on the right of each set of graphs, $t = 0$ (black continuous curves), $t = 0.5$ (black dashed curves), and $t = 1$ (blue continuous curves), are calculated for $p = 0$ (no phase noise present). The curves that correspond to the remaining three labels, $t = 0$ (black continuous curves), $t = 0.5$ (black dotted curves), and $t = 1$ (blue continuous curves), are calculated for $p = 1$ (100% dephasing present). In this case, the displacement between $t = 0$ and $t = 1$ is $2\pi/3$. Now, the visibility does not become null under 100% dephasing.

with $d > 2$, although there is no complete recovery of the initial visibility when the cyclic $\mathrm{SU}(d) \otimes \mathrm{SU}(d)$ operation is completed, the $2\pi/d$ phase shift is evident from both the equations shown in Table II and the graphs shown in Figs. 3(b) and 4(b). On the other hand, the visibility of the interference patterns is almost zero when the operation is realized in the presence of 100% dephasing ($p = 1$).

Finally in Fig. 5 we plot the visibilities of the interference patterns for maximally entangled and product states obtained from the coincidence expressions presented in Table II as a function of the dephasing weight represented by the parameter p. Note that the expressions for $t = 0$ are identical for maximally entangled and product states.

VI. CONCLUSION

We demonstrate the robustness of fractional topological phases in two-qudit states under local $\mathrm{SU}(d)$ operations in a dephasing environment. A photonic experimental proposal is presented where the fractional topological phases are measured on two-photon interference. The two-qudit states are encoded in the transverse modes of entangled photon pairs generated by spontaneous parametric down-conversion. The $\mathrm{SU}(d) \otimes \mathrm{SU}(d)$ and dephasing operations are applied to the transverse photon path variables, which can be realized with a spatial light modulator. The dephasing process is included by using the corresponding Kraus operators. The two-photon
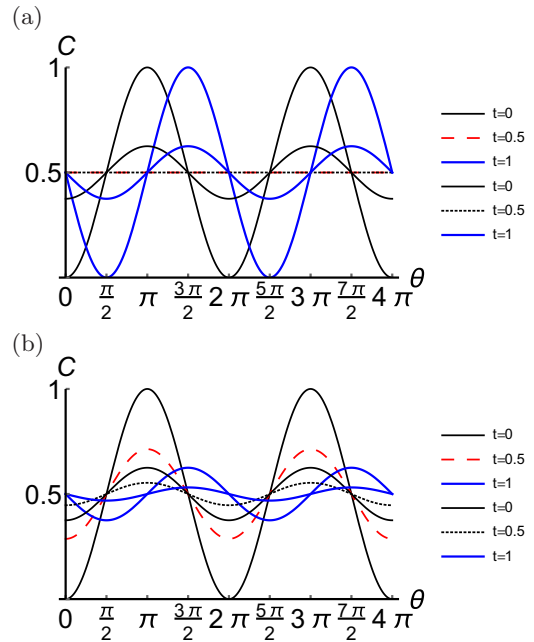
(a)

(b)

FIG. 4. Situation analogous to Fig. 2 for two-ququart states: (a) maximally entangled state and (b) product state. The curves that correspond to the first three labels shown on the right of each set of graphs, $t = 0$ (black continuous curves), $t = 0.5$ (red dashed curves), and $t = 1$ (blue continuous curves), are calculated for $p = 0$ (no phase noise present). The curves that correspond to the remaining three labels, $t = 0$ (black continuous curves), $t = 0.5$ (black dotted curves), and $t = 1$ (blue continuous curves), are calculated for $p = 1$ (100% dephasing present). In this case, the displacement between $t = 0$ and $t = 1$ is $\pi/2$. Again, the visibility does not become null under 100% dephasing.
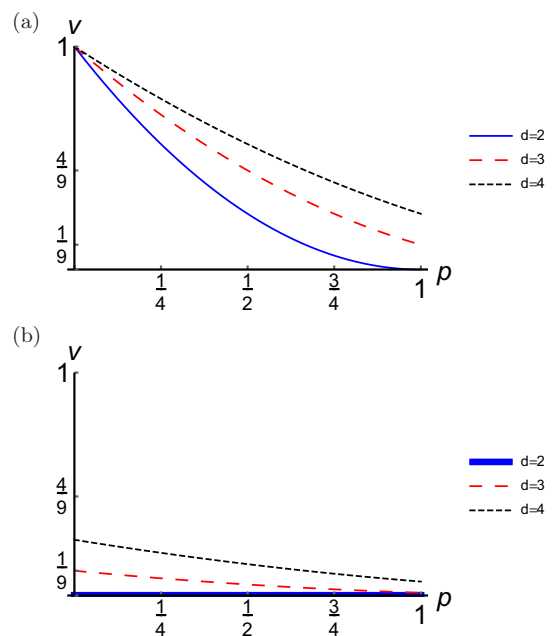
(a)

(b)

FIG. 5. (a) Visibilities (v) of the interference patterns for the two-qudit maximally entangled states ($d = 2$, 3, or 4) in terms of the dephasing parameter p. (b) Visibilities (v) of the interference patterns for the two-qudit product states ($d = 2$, 3, or 4) in terms of the dephasing parameter p. Expressions are shown in Table II.

interference allows us to determine the fractional topological phases through the shift of the interference fringes as the cyclic operation is completed. Topological phase robustness is predicted even for 100% dephasing for two-qudit systems with $d > 2$. This fact suggests that the fractional topological phase can be a useful tool for quantum phase gate implementations under the action of dephasing environments. Another interesting subject that remains to be understood is the role played by fractional topological phases in quantum phase transitions. The scaling of geometric phases in quantum phase transitions of spin chains has already been discussed in the literature [31–33]. Meanwhile, the occurrence of fractional topological phases in multiple-qubit systems have already been investigated [34]. Therefore, the connection between fractional topological phases and quantum phase transitions offers a natural course of future research.

[1] P. Milman and R. Mosseri, Phys. Rev. Lett. **90**, 230403 (2003).

[2] W. LiMing, Z. L. Tang, and C. J. Liao, Phys. Rev. A **69**, 064301 (2004).

[3] F. D. Zela, J. Opt. B: Quantum Semiclassical Opt. **7**, 372 (2005).

[4] P. Milman, Phys. Rev. A **73**, 062118 (2006).

[5] C. E. R. Souza, J. A. O. Huguenin, P. Milman, and A. Z. Khoury, Phys. Rev. Lett. **99**, 160401 (2007).

[6] J. Du, J. Zhu, M. Shi, X. Peng, and D. Suter, Phys. Rev. A **76**, 042121 (2007).

[7] J. C. Loredo, M. A. Broome, D. H. Smith, and A. G. White, Phys. Rev. Lett. **112**, 143603 (2014).

[8] L. E. Oxman and A. Z. Khoury, Phys. Rev. Lett. **106**, 240503 (2011).

[9] A. Z. Khoury and L. E. Oxman, Phys. Rev. A **89**, 032106 (2014).

[10] A. Z. Khoury, L. E. Oxman, B. Marques, A. Matoso, and S. Pádua, Phys. Rev. A **87**, 042113 (2013).

[11] A. A. Matoso, X. Sánchez-Lozano, W. M. Pimenta, P. Machado, B. Marques, F. Sciarrino, L. E. Oxman, A. Z. Khoury, and S. Pádua, Phys. Rev. A **94**, 052305 (2016).

[12] A. A. Matoso, R. A. Ribeiro, L. E. Oxman, A. Z. Khoury, and S. Pádua, Sci. Rep. **9**, 577 (2019).

[13] A. Carollo, I. Fuentes-Guridi, M. F. Santos, and V. Vedral, Phys. Rev. Lett. **90**, 160402 (2003).

[14] M. Amniat-Talab and H. R. Jahromi, P. R. Soc. London, Ser A **469**, 20120743 (2013).

[15] P. Solinas, P. Zanardi, and N. Zanghì, Phys. Rev. A **70**, 042316 (2004).

[16] C. Lupo and P. Aniello, Phys. Scr. **79**, 065012 (2009).

[17] P. Zanardi and M. Rasetti, Phys. Lett. A **264**, 94 (1999).

[18] J. A. Jones, V. Vedral, A. Ekert, and G. Castagnoli, Nature (London) **403**, 869 (2000).

[19] L.-M. Duan, J. I. Cirac, and P. Zoller, Science **292**, 1695 (2001).

[20] P. Solinas, P. Zanardi, N. Zanghì, and F. Rossi, Phys. Rev. B **67**, 121307 (2003).

[21] Z. N. Gürkan and E. Sjöqvist, Phys. Lett. A **379**, 3050 (2015).

[22] E. Sjöqvist, Phys. Lett. A **380**, 65 (2016).

[23] A. C. Lobo, R. A. Ribeiro, C. de Assis Ribeiro, and P. R. Dieguez, Eur. J. Phys. **33**, 1063 (2012).

[24] L. E. Oxman, A. Z. Khoury, F. C. Lombardo, and P. I. Villar, Ann. Phys. **390**, 159 (2018).

[25] B. Marques, A. Matoso, W. Pimenta, A. J. Gutiérrez-Esparza, M. Santos, and S. Pádua, Sci. Rep. **5**, 16049 (2015).

[26] Y. Aharonov and J. Anandan, Phys. Rev. Lett. **58**, 1593 (1987).

[27] M. Berry, Proc. R. Soc. London, Ser. A **392**, 45 (1984).

[28] L. Neves, G. Lima, E. J. S. Fonseca, L. Davidovich, and S. Pádua, Phys. Rev. A **76**, 032314 (2007).

[29] K. Kraus, Ann. Phys. **64**, 311 (1971).

[30] T. Yu and J. H. Eberly, Phys. Rev. B **68**, 165322 (2003).

[31] S.-L. Zhu, Phys. Rev. Lett. **96**, 077206 (2006).

[32] L. Campos Venuti and P. Zanardi, Phys. Rev. Lett. **99**, 095701 (2007).

[33] A. Carollo, B. Spagnolo, and D. Valenti, Sci. Rep. **8**, 9852 (2018).

[34] M. Johansson, M. Ericsson, K. Singh, E. Sjöqvist, and M. S. Williamson, Phys. Rev. A **85**, 032112 (2012).